Induction Heating of Firebricks for the Large-Scale Storage of Nuclear and Renewable Energy

by

Richard T. Ibekwe

Submitted to the
Department of Nuclear Science and Engineering
and to the
Department of Mechanical Engineering
in Partial Fulfillment of the Requirements for the Degree of

Bachelor of Science in Nuclear Science and Engineering
and in Mechanical Engineering
at the

Massachusetts Institute of Technology

June 2018

Signature of Author: _____

Department of Nuclear Science and Engineering
Department of Mechanical Engineering
May 11, 2018

Certified by: _____

Charles Forsberg
Principal Research Scientist, Nuclear Science and Engineering
Thesis Supervisor

Certified by: _____

Ahmed Ghoniem
Professor of Mechanical Engineering
Thesis Supervisor

Accepted by: _____

Michael Short
Assistant Professor of Nuclear Science and Engineering
Undergraduate Chair

Accepted by: _____

Rohit Karnik
Professor of Mechanical Engineering
Undergraduate Officer

Induction Heating of Firebricks for the Large-Scale Storage of Nuclear and Renewable Energy

by

Richard T. Ibekwe

Submitted to the Department of Nuclear Science and Engineering
on May 18, 2018
and to the Department of Mechanical Engineering
on May 11, 2018
in Partial Fulfillment of the
Requirements for the Degree of

Bachelor of Science in Nuclear Science and Engineering
and in Mechanical Engineering

Abstract

The lack of low-cost, large-scale energy storage is one of the biggest obstacles to the ongoing transition from an energy market dominated by fossil fuels to one dominated by nuclear and renewable energy. Storing energy as heat in firebricks has a number of potential advantages over existing energy storage methods such as batteries and pumped-storage.

This work investigated the application of induction heating to firebrick energy storage. The distributions of magnetic field and temperature in firebricks under induction heating were simulated and compared with experiments. It was found that firebricks can be induction heated to high temperatures (>700°C); different material compositions give different temperature responses; and rate of temperature increase is positively correlated with electrical conductivity. It was also shown that, in addition to use in large-scale energy storage, induction heating can be used to measure electrical conductivity and for firebrick quality assurance.

Thesis Supervisor: Charles Forsberg
Title: Principal Research Scientist, Nuclear Science and Engineering

Thesis Supervisor: Ahmed Ghoniem
Title: Professor of Mechanical Engineering

Acknowledgments

I am particularly thankful to Charles Forsberg and Ahmed Ghoniem for their advice and support throughout the course of this work. Richard Lanza and Nuno Loureiro have also provided useful insights, for which I am grateful. I thank Daniel Stack for his help and ideas at various points during this research.

I thank Shaymus Hudson for his patient hours of work in helping me conduct the induction heating experiments, and Mike Tarkanian and Tara Fadenrecht for giving me access to the Materials Processing Laboratory's induction furnace with which these experiments were performed. I thank Bill Cormier for his support in preparing the firebrick samples for the experiments. I would also like to thank Amy Carleton and Jane Kokernak for their help with writing and refining this thesis.

I also thank HarbisonWalker International for providing the firebrick samples used in these experiments and Exelon for providing the funding.

Table of Contents

List of Figures

List of Tables

1 Introduction

The lack of low-cost, large-scale energy storage is one of the biggest obstacles to the ongoing transition from an energy market dominated by fossil fuels to one dominated by nuclear and renewable energy. The supply of electricity from solar and wind power fluctuates significantly and unpredictably, and the low operating costs of solar and wind power cause the collapse of the price of electricity during periods of high supply. Storing the electricity from nuclear and renewable energy when demand is low and supply is high for later release would stabilize the supply and price of electricity (Schmalensee 2015).

For many years, the most popular energy storage technologies have been batteries and pumped-storage dams. The main disadvantages of these systems are their high cost and poor scalability. Heating firebricks to high temperatures is a promising alternative energy storage technology. Air can then be blown through the hot firebrick to provide hot air for industrial furnaces and gas turbines. A firebrick is a type of brick used mainly as the lining of furnaces because of its heat-resistant properties. The high heat capacity, density and melting point of firebricks would give a firebrick system a volumetric energy density comparable to that of lithium-ion batteries. In addition, the high abundance and low cost of the firebrick materials suggest that a firebrick system would be up to two orders of magnitude less expensive than lithium-ion batteries, and significantly more scalable and widely deployable than pumped-storage dams (Forsberg et al. 2017).

The large-scale storage of energy as heat in firebricks is the development of an old idea. Domestic-scale firebrick energy storage was popular in Britain and Germany in the 1960s, where a total of more than 100,000 MWh of such heat storage capacity was installed (Mohr 1970). Small firebrick systems (less than 100 kWh each) were distributed to households to time-shift some electricity use from day to night for home heating. This reduced the burden on baseload power stations during the day, smoothing the daily national power consumption oscillations and reducing peak national power requirements (Price 2011).

Previous work has focused mainly on establishing the economic case for firebrick heat storage and determining the basic technical requirements of such a system (Forsberg et al. 2017). The method chosen for heating the firebricks will depend on the desired operating temperature and cost of the system. For low temperatures, there are many heating options, including gas combustion, resistance heating (< 1000°C) and heat exchangers with heat provided by a nuclear reactor. At the very high temperatures (~1800°C) proposed for the firebrick heat storage system, these options

are either technologically infeasible or prohibitively expensive—yet there are large incentives to develop such high-temperature heat storage technologies. Cold air can be blown through shafts in the firebrick to provide hot air needed to produce cement, glass, or building brick. If integrated into a combined cycle natural gas turbine, electricity can be converted to stored heat at times of low electricity demand and replace the use of natural gas at times of high electricity demand. In the longer-term such a firebrick energy storage system can be coupled to a Nuclear air-Brayton Combined Cycle (NACC) plant that operates in two modes; baseload and peak load with added power produced by natural gas or the firebrick energy storage system.

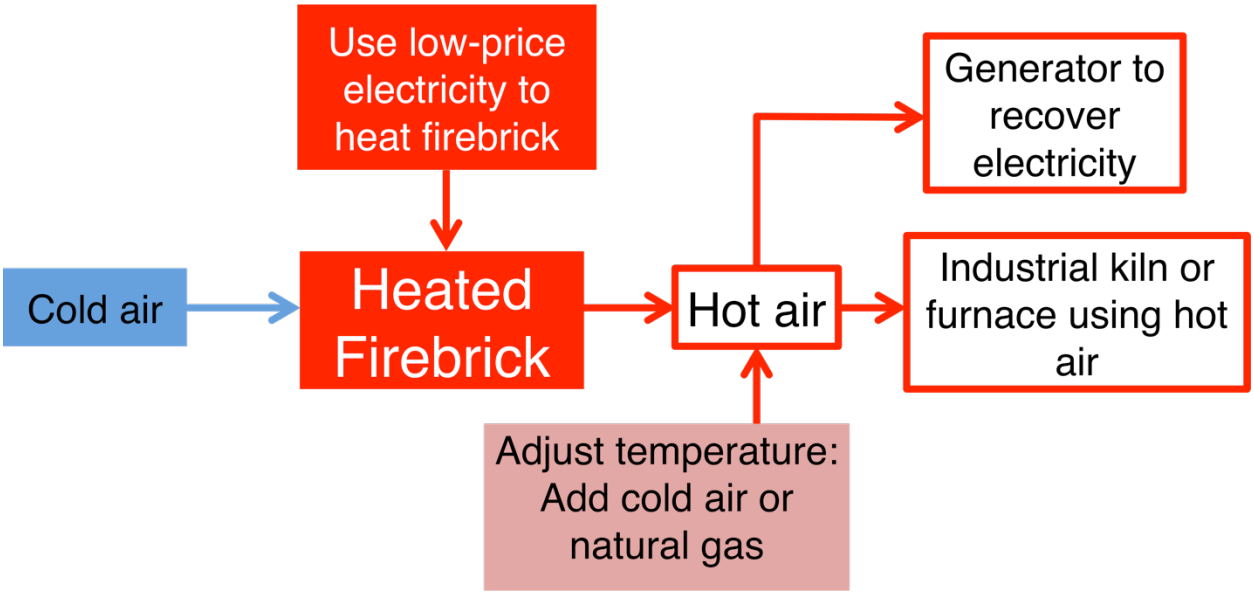

Figure 1: Schematic diagram of a firebrick energy storage system.

The only viable heating methods at these and higher temperatures are electric resistance heating or induction heating, which heats the firebrick with the current induced by a changing magnetic field in the material. Each has its own technology challenges. The possible temperature of an induction-heated system is effectively unlimited and for this reason induction heating is used extensively in industry for melting high-melting-temperature materials such as glass and tungsten (Deshmukh 2005). Patents (Balordi 1980; Virgin 1985) exist for induction heaters to provide hot air and steam for home heating, but they are limited to relatively low temperatures (650°C) because of the use of metal rather than ceramic cores. This work describes the design of a hypothetical

induction-heated firebrick energy storage system; models the eddy currents, heat and temperature distributions and time evolutions in the system; and investigates the effect of different firebrick material compositions. It also describes new applications of induction heating as a way of estimating the electrical conductivity of firebrick materials and for firebrick quality assurance.

2 Background

2.1 Induction heated firebrick energy storage design concepts

The firebrick energy storage system consists of a configuration of high-density, high-heat capacity ceramic firebricks that stores electricity as high-temperature heat during periods of low or negative electricity prices, where "low" means electricity prices below that from competing fossil fuels (Forsberg et al. 2017). The heat can later be recovered by pumping air through channels in the hot firebrick energy storage medium. The hot air may be used directly in industrial processes or it may be converted back into electricity to be used for increasing the output of a power plant such as a nuclear reactor.

Three design concepts are proposed, as shown in Fig. 2. (a) In the first concept, the firebrick energy storage system consists of a core of electrically conductive firebrick surrounded by a sheath of electrically insulating firebrick. An induction coil encircles the whole system. The electrically conductive firebrick is Joule heated by eddy currents generated by the magnetic field in the volume enclosed by the induction coil (see Section 3.1). (b) The second concept is similar to the first, except that the induction coil is embedded in a shaft in the center of the firebrick energy storage medium and the firebrick is heated by eddy currents generated by the magnetic field outside the volume enclosed by the induction coil. (c) In the third concept, the main firebrick energy storage medium is not directly induction heated. Instead, a smaller firebrick unit separate from the main storage medium is induction heated; air is heated by pumping it through this unit; the hot air is carried by insulated pipes to the main storage medium, where the heat is transferred to the firebrick through air channels.

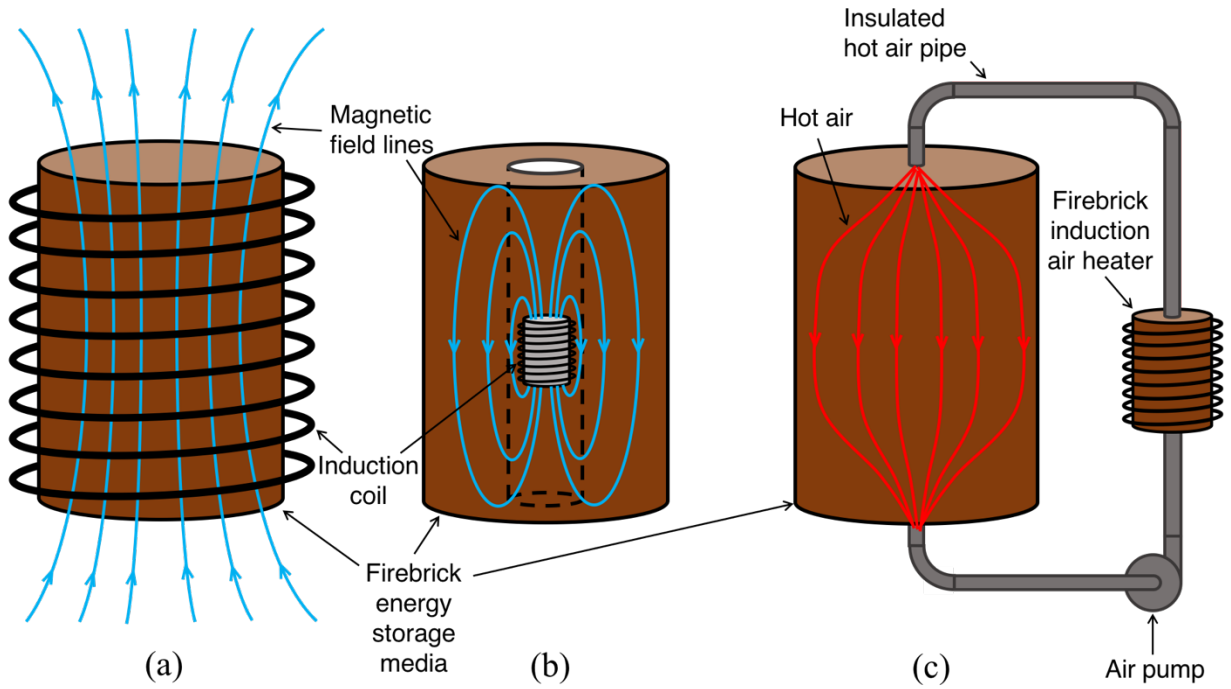

Figure 2: Three proposed design concepts for an induction-heated firebrick energy storage system. (a) A large induction coil surrounds the entire firebrick energy storage medium; the firebrick is heated by the magnetic field generated inside the coil. (b) A small induction coil is embedded in the firebrick energy storage medium; the firebrick is heated by the magnetic field generated outside the coil. (c) An induction coil heats a small mass of firebrick, which acts as an air heater; hot air is pumped to a larger firebrick energy storage medium, to which heat is transferred through air channels.

2.2 Existing firebrick energy storage technology

2.2.1 Firebrick Resistance-heated Energy Storage

The main large-scale firebrick electric heat storage technology currently being developed is MIT's Firebrick Resistance-heated Energy Storage (FIRES), described in detail in Forsberg et al. (2017), which resistance heats the firebrick energy storage medium with an applied electric current. FIRES has a maximum operating temperature of ~1800°C and a typical temperature range of ~1000°C, giving a heat storage capacity of 0.5–1 MWh/m^3. At these very high temperatures, standard resistance heating elements made of nichrome wire and similar materials degrade quickly through oxidation; instead, electric current is applied directly through a firebrick energy storage medium composed of firebrick with relatively high electrical conductivity such as silicon carbide, which

acts as the heating element. The cost of FIRES would be as low as $5/kWh, substantially less expensive than batteries.

The main advantages of an induction-heated firebrick energy storage system over a resistance-heated system such as FIRES are potentially higher power density and consequently higher heating rate; higher operating temperature; and the fact that the induction coils do not contact the firebrick, meaning that the electrical and thermal systems are separate, which would make installation and maintenance more straightforward and potentially less expensive.

2.2.2 Firebrick recuperators

Historically, the main large-scale industrial application of firebrick energy storage has been in heat recuperators and regenerators in a range of industrial processes to recover and reuse heat that would otherwise be lost. In an open-hearth steel mill, two recuperators alternately store heat and supply high-temperature air for steelmaking. In the steelmaking process, steel with a low carbon content is produced from pig iron with a high carbon content. Hot air is blown over a molten bath of pig iron (with a temperature of ~1600°C) to oxidize the carbon. The hot exhaust gas produced is passed through one of the firebrick recuperators, which heats up as the exhaust gas cools before being expelled through the stack. When the firebrick recuperator is hot, the fans are reversed, blowing cold air through them. The cold air is heated by the recuperator and its temperature is raised further by burning fuel. The hot air is blown over the molten pig iron and is passed through the second recuperator, before being expelled through the stack. This alternating energy storage process is repeated and saves large amounts of energy by reducing the temperature range through which incoming air must be heated with fuel. (Ibekwe and Forsberg 2015)

3 Methods

3.1 Induction heating theory

An induction-heated system consists of an electrically conductive workpiece surrounded by an induction coil carrying an alternating electric current. The alternating current in the coil generates a magnetic field that penetrates and induces alternating eddy currents in the workpiece. These eddy currents dissipate heat in the workpiece by Joule heating. The temperature distribution in the workpiece is governed by power input from the eddy currents and power loss through conductive, convective and radiative heat transfer within and on the surface of the workpiece. In a firebrick energy storage system, the workpiece is composed of firebrick.

Eddy current distribution and consequent power dissipation are found by solving Maxwell's equations (described in detail in Section 3.2) in the firebrick. Using a similar method to that found in Gresho and Derby (1987) and Tavakoli et al. (2009), we assume that (i) all materials in the system are linear, isotropic and have no net electric charge, (ii) the system is rotationally symmetric about the z-axis, that is, the firebrick is cylindrical and all quantities are independent of the azimuthal coordinate ϕ, (iii) the displacement current is negligible (it is only significant when the electromagnetic wavelength is comparable to or smaller than the length of the system; in these experiments, the wavelength is ~130 km at the induction furnace frequency of 2300 Hz, much greater than the system size of ~15 cm). Maxwell's equations become:

$$\nabla \cdot \mathbf{E} = 0, \tag{1}$$

$$\nabla \cdot \mathbf{B} = 0, \tag{2}$$

$$\nabla \times \mathbf{B} = \mu \mathbf{J}, \tag{3}$$

$$\nabla \times \mathbf{E} = -\frac{\partial \mathbf{B}}{\partial t}, \tag{4}$$

$$\mathbf{J} = \sigma \mathbf{E}, \tag{5}$$

Solving Eqs. 1 – 5 will yield the dissipated power, given by

$$P = \mathbf{J} \cdot \mathbf{E} = \sigma E^2 \tag{6}$$

where P is the power per unit volume dissipated in the firebrick, a function of space and time.

We can introduce a vector potential **A** such that

$$\mathbf{B} = \nabla \times \mathbf{A}, \tag{7}$$

which, using our assumption that the system is rotationally symmetric and further assuming that the helicity or pitch of the induction coil is zero (that is, that currents in the coil and eddy currents in the firebrick flow only in the azimuthal direction, so that $\mathbf{J} = \mathbf{e}_\phi \mathrm{J}_\phi$), allows Eqs. 1 – 5 to be transformed into the scalar equation (Gresho and Derby 1987):

$$\frac{\partial}{\partial r}\left(\frac{1}{r}\frac{\partial \psi}{\partial r}\right) + \frac{\partial}{\partial z}\left(\frac{1}{r}\frac{\partial \psi}{\partial z}\right) = -\mu J_\phi \ , \tag{8}$$

where (r, ϕ, z) are the cylindrical coordinates, ψ is a magnetic stream function given by $\psi(r,z,t) \equiv rA_\phi(r,z,t)$ and A_ϕ is the azimuthal component of the vector potential **A**.

Assuming a sinusoidal AC driving current in the coil given by

$$J_\phi = J_0 \cos \omega t \tag{9}$$

where J_0 is the amplitude of the driving current and ω is the frequency, and eddy currents in the firebrick given by

$$J_\phi = -\frac{\sigma}{r}\frac{\partial \psi}{\partial t}$$

yields a solution of the form

$$\psi(r,z,t) = C(r,z)\cos \omega t + S(r,z)\sin \omega t, \tag{10}$$

where $C(r,z)$ is the in-phase component and $S(r,z)$ is the out-of-phase component of the solution.

Substituting $C(r,z)$ and $S(r,z)$ for ψ into Eq. 8 yields a set of coupled partial differential equations:

$$\frac{\partial}{\partial r}\left(\frac{1}{r}\frac{\partial C}{\partial r}\right) + \frac{\partial}{\partial z}\left(\frac{1}{r}\frac{\partial C}{\partial z}\right) = \begin{cases} -\mu\left(J_0 - \frac{\sigma\omega}{r}S\right) & \text{in the coil,} \\ \frac{\mu\sigma\omega}{r}S & \text{in the firebrick,} \\ 0 & \text{elsewhere,} \end{cases} \tag{11}$$

$$\frac{\partial}{\partial r}\left(\frac{1}{r}\frac{\partial S}{\partial r}\right) + \frac{\partial}{\partial z}\left(\frac{1}{r}\frac{\partial S}{\partial z}\right) = \begin{cases} -\frac{\mu\sigma\omega}{r}C & \text{in the coil,} \\ -\frac{\mu\sigma\omega}{r}C & \text{in the firebrick,} \\ 0 & \text{elsewhere,} \end{cases} \tag{12}$$

where μ takes the values μ_0 (permeability of free space) and μ_f (permeability of the firebrick) in the coil and firebrick, respectively; σ takes the values σ_c (conductivity of the coil) and σ_f (conductivity of the firebrick) in the coil and firebrick, respectively. $\delta \equiv \sqrt{(2/\mu\sigma\omega)}$ is called the

skin depth, a measure of the magnetic field penetration into the firebrick. The boundary conditions for Eqs. 11 and 12 are $C = S = 0$ in the far-field ($r, z \to \infty$) and at the axis of symmetry ($r = 0$).

After solving for $C(r,z)$ and $S(r,z)$, the eddy current distribution is given by

$$J_\phi = -\frac{\sigma}{r}\frac{\partial \psi}{\partial t} = \frac{\sigma\omega}{r}[C(r,z)\sin\omega t - S(r,z)\cos\omega t], \tag{13}$$

power dissipation per unit volume is given by

$$P(r,z,t) = \frac{J_\phi^2}{\sigma} = \frac{\sigma\omega^2}{r^2}(S\cos\omega t - C\sin\omega t)^2, \tag{14}$$

and the volumetric heat generation rate is given by

$$q(r,z) = \frac{\omega}{2\pi}\int_0^{2\pi/\omega} P(r,z,t)\,dt = \frac{\sigma\omega^2}{2r^2}(C^2 + S^2), \tag{15}$$

which is the source term of the heat equation

$$\frac{\partial T}{\partial t} - \alpha\nabla^2 T = q(r,z), \tag{16}$$

where T is the temperature at a given point in time and space, and α is the thermal diffusivity. Solving this equation yields the temperature distribution in the firebrick.

3.2 Maxwell's equations

Electric charges generate electric fields. The relationship between electric charges and their resulting fields was formulated by Joseph-Louis Lagrange in 1773 and Carl Friedrich Gauss in 1813, a relationship typically referred to as Gauss's law, which states that the electric flux out of a closed surface is proportional to the net charge enclosed within the surface:

$$\nabla \cdot \mathbf{E} = \frac{\rho}{\varepsilon} \tag{17}$$

where **E** is the electric field intensity, ρ is the net electric charge density and ε is the permittivity of the material.

There is no net magnetic flux out of any closed surface, meaning that there are no "magnetic charges" or monopoles. This is expressed in Gauss's law for magnetism:

$$\nabla \cdot \mathbf{B} = 0 \tag{18}$$

where **B** is the magnetic flux density.

In 1820, Hans Christian Ørsted observed that a current-carrying wire deflected a compass needle, demonstrating that electric currents generate magnetic fields. An expression for the

magnetic field around an electric current was derived by James Clerk Maxwell in 1861. This relation is typically called Ampère's law:

$$\nabla \times \mathbf{B} = \mu\left(\mathbf{J} + \varepsilon\frac{\partial \mathbf{E}}{\partial t}\right) \tag{19}$$

where $\mathbf{J}$ is the free charge current density and the quantity $\varepsilon\frac{\partial \mathbf{E}}{\partial t}$ is the displacement current density.

In 1831, Michael Faraday observed that, with two insulated wire coils wrapped around an iron ring, opening and closing a switch connecting a battery to one of the coils induced a momentary current in the other coil; with the switch closed and a steady current flowing through one coil, there was no current detected in the other coil. He concluded that the changing magnetic field generated by one of the coils induced current in the other coil, which with a refinement by Heinrich Lenz became Faraday's law of induction:

$$\nabla \times \mathbf{E} = -\frac{\partial \mathbf{B}}{\partial t} \tag{20}$$

The relation between free charge current density and electric field intensity is given by Ohm's law:

$$\mathbf{J} = \sigma\mathbf{E} \tag{21}$$

where σ is the electrical conductivity, which is a function of temperature.

Collectively, Eqs. 17 – 21 are referred to as Maxwell's equations.

3.3 Applications of induction heating

In the decades after Faraday's discovery, induction was used to design transformers for changing the voltage in circuits and more efficiently transmitting electricity. Heat was produced as a byproduct in the magnetic core of the transformer; the cores were composed of laminated stacks of steel to reduced heating, but it was later realized that the heating effect could be used for melting and heat-treating metal. Rudnev et al. (2002) describes in detail the various applications of induction heating.

Induction heating is used for various metallurgical heat treatment processes, especially for steels and cast irons (e.g., hardening, tempering, normalizing, annealing, spheroidizing and sintering). In surface and through hardening, a metal workpiece is heated to and held at a critical temperature (727°C in cast iron) that causes a change in crystal structure at the surface or throughout the

workpiece; the workpiece is then rapidly cooled ("quenched"); the process of heating and cooling transforms the microstructure of the metal to a much harder form, which can greatly improve the wear-resistance of parts such as tools and gears. The hardening process typically also increases the brittleness of the workpiece; to reduce brittleness and improve other properties, the workpiece may be sintered: the workpiece is inductively reheated to some temperature below the critical temperature (this may be anywhere in the range of 120°C to 600°C), then allowed to cool in air. Normalizing, annealing and spheroidizing similarly cause microstructural changes that improve the mechanical properties of metal.

Induction mass heating is used to heat metals to high temperatures that allow metal forming (e.g., forging, rolling and extruding) or provide heat for coating operations (e.g., curing paints and galvanizing). At higher temperatures, induction heating is used for melting metal (e.g., melting ore during the metalmaking process, or melting metal for use in casting). Induction heating may also be used to weld two metal workpieces together. Induction hardening, mass heating and melting typically use relatively low induction frequencies (anywhere between 200 Hz and 30 kHz), while induction welding uses relatively high frequencies (200 kHz to 600 kHz).

Two patents (Balordi 1980; Virgin 1985) describe low-frequency (both 60 Hz), low voltage (12 V and 110 V, respectively) induction heaters for heating air or water. The first uses an induction-heated steel core to heat air to 650°C for use in thermally sealing poly-coated paper; the second uses induction-heated "magnetizable steel balls" to provide steam or hot air for home heating. At these low temperatures, metal is sufficient as core material; at higher temperatures (above 1000°C), any metal will be oxidized, necessitating the use of ceramic firebricks in a system similar to those described in Section 2.1, which this work is investigating.

3.4 Experimental setup

An Inductotherm furnace with Power-Trak 75-30 R power supply was used for heating the firebrick samples in these experiments. The power supply delivered electrical power to the induction coil around the furnace crucible with a maximum power rating of 75 kW at a fixed frequency of 2300 Hz. In practice, the power supply delivered a maximum power of approximately 55 kW at 2300 Hz with a voltage of 900 V. The crucible was composed of clay graphite ceramic and measured 194 mm in inner diameter. The induction coil consisted of 14 turns, was composed

of copper with a total mass of 50 kg and measured 267 mm in inner diameter and 308 mm in total height.

The firebricks used were cylinders manufactured by HarbisonWalker International. The cylindrical geometry was used because the eddy currents in the firebrick flow azimuthally and all other quantities are azimuthally symmetry (see Section 3.1). Seven different firebrick compositions were used, as listed in Table 2. Three of the bricks (TZB, HARBIDE, NISIC 20) were manufactured by pressing and sintering to 800°C ceramic powder to form cuboid bricks that were then cut into cylinders with a diameter of 95 mm and height of 51 mm or 76 mm. The other four bricks (SHOT-TECH SIC 80, GREENCAST-90 RB ON-LINE, THOR 60 ADTECH, SERV 95) were manufactured by casting and firing to 800°C ceramic slurry, which allowed them to be formed directly into cylinders with a diameter of 127 mm and height of 152 mm.

In each experiment, a cylindrical firebrick sample was placed in the center of the floor of the furnace crucible; the firebrick sample was inductively heated and its surface temperature measured with an infrared camera suspended directly above the center of the sample. The minimum temperature that the infrared camera could measure was 92°C (365 K). The temperature was recorded at 10-second intervals until the firebrick sample reached either 727°C (1000 K) or a lower steady temperature. A schematic diagram of the experimental setup is shown in Fig. 3. A detailed technical drawing of the furnace supplied by the manufacturer is shown in Fig. 16 and a circuit diagram of the power supply is shown in Fig. 17.

Future work would investigate the effect of varying the frequency of the current in the induction coil, with a particular focus on a large-scale system's performance at the 60 Hz line frequency. A 60 Hz input would likely be less expensive to produce at large scale than higher frequencies but, since power is proportional to the square of frequency (see Eq. 14), would require a larger current to maintain the same power.

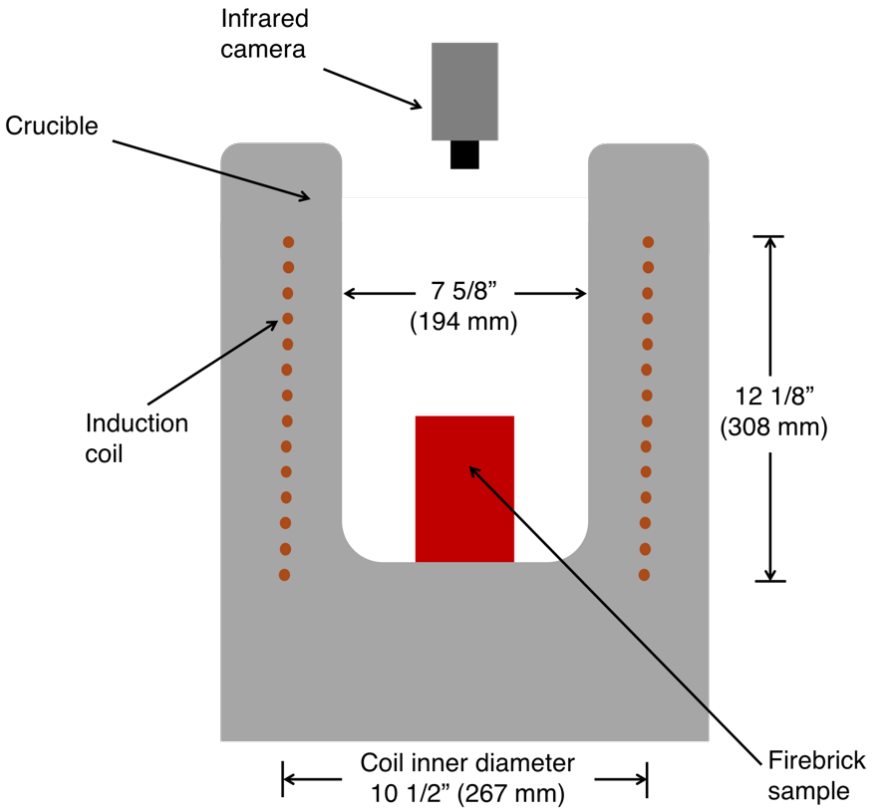

Figure 3: Schematic diagram of experimental setup (cross-section viewed from the side).

In addition to using the infrared camera to measure surface temperature, it was originally intended that the internal temperature of the firebrick would be measured at a number of positions with K-type thermocouples. However, it proved exceptionally difficult to drill into the firebrick samples, because the drill bits wore out very quickly from abrasion with the firebricks. Table 1 shows the Mohs hardness (which measures the ability of one material to scratch another) of various materials; when two materials are in contact, the material with the higher Mohs hardness is able to scratch the other material. The materials of which the firebricks were composed all have high Mohs hardness. 1/4-inch high-speed steel, tungsten carbide and diamond-coated carbide drill bits were all incapable of forming shafts in the firebrick for the thermocouples: even when attempting to drill into materials with lower Mohs hardness than the drill bit material, the drill bits experienced rapid wear and quickly became blunt and ineffective. Fig. 4 shows a diamond-coated drill bit before and after a single attempt to use it to drill shafts in the firebrick samples; the significant wear on the drill bit is apparent. In future work, the bricks would be manufactured with metal rods of the diameter of the thermocouples place into the bricks while still a slurry or powder; the metal could then be easily drilled through to form the thermocouple shafts after curing.

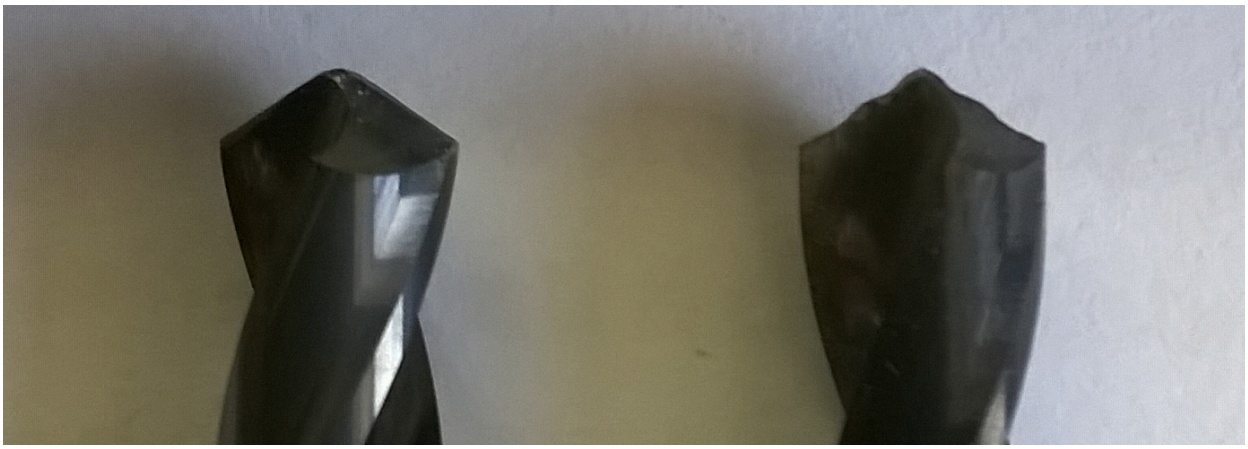

Figure 4: 1/4-inch diamond-coated carbide drill bits before (left) and after (right) attempting to form shafts in the firebrick samples for insertion of temperature probes. Notice the significant wear in the edge of the drill bit from a single use, demonstrating the high hardness of the firebrick.

Material	**Mohs hardness**
Mild steel	4–4.5
Glass	5.5
Hematite (Fe_2O_3)	6–7.5
Silica (SiO_2)	7
High-speed steel	7.5
Zirconia (ZrO_2)	8
Chromia (Cr_2O_3)	8–8.5
Silicon nitride (Si_3N_4)	8.5
Alumina (Al_2O_3)	9
Tungsten carbide (WC)	9
Silicon carbide (SiC)	9–9.5
Diamond	10

Table 1: Mohs scratch hardness of various materials (Samsonov 1968). The firebrick samples were composed of various combinations of the materials listed in normal typeface. Drill bits composed of the materials in bold italic typeface were used to attempt to drill into the firebricks, but were incapable of doing so, even when their hardness was higher than that of the firebrick materials. Two other materials are shown in italic typeface for comparison.

Firebrick	Material composition (weight % of each)	Bulk density (g/cm^3)	Diameter (mm)	Height (mm)	Manufacturing technique
GREENCAST-90 RB ON-LINE	Al_2O_3 (88.2), Fe_2O_3 (5.3), CaO (4.5), SiO_2 (0.8), Na_2O (0.3)	2.55	127	152	Cast and fired at 800°C
HARBIDE	SiC (85.4), SiO_2 (11.1), Al_2O_3 (2.0), other oxides (0.6)	2.66	95	51	Pressed and sintered at 800°C
NISIC 20	SiC (77.0), Si_3N_4 (20.5), Al_2O_3 (1.2), CaO + MgO (1.0), Fe_2O_3 (0.3)	2.67	95	76	Pressed and sintered at 800°C
SERV 95	Cr_2O_3 (92.2), Al_2O_3 (5.1), TiO_2 (1.1), others (1.6)	3.73	127	152	Cast and fired at 800°C
SHOT-TECH SIC 80	SiC (78.0), SiO_2 (10.5), Al_2O_3 (8.3), CaO (2.7), Fe_2O_3 (0.3), Na_2O + K_2O (0.2)	2.37	127	152	Cast and fired at 800°C
THOR 60 ADTECH	SiC (62.1), Al_2O_3 (20.6), SiO_2 (14.7), CaO (2.2), Fe_2O_3 (0.2), Na_2O + K_2O (0.2)	2.51	127	152	Cast and fired at 800°C
TZB	ZrO_2 (66.0), SiO_2 (32.0), other oxides (2.0)	3.77	95	76	Pressed and sintered at 800°C

Table 2: Technical data of the various firebricks used in these experiments. The firebricks were supplied by HarbisonWalker International; the names and data are those provided by the same.

3.5 Firebrick conductivity

A material of particular interest as a main constituent of induction-heated firebrick is silicon carbide, because of the high electrical conductivity reported in Deshmukh (2005) (see Fig. 5). However, Chiochetti and Henry (1953) report a significantly lower conductivity (see Fig. 5). This large disparity in electrical conductivity is not unusual: the presence of small quantities of impurities, differences in the way in which the samples are prepared and differences in grain sizes can all have a large effect on measured conductivity (Hensler and Henry 1953). Therefore, the conductivities of the samples used in the experiments (see Table 2) are not known *a priori*. The induction heating experiments in this work present a new way of measuring the conductivity of

firebricks, by allowing temperature response simulations using various inputted conductivities to be compared and correlated with experimental temperature response measurements.

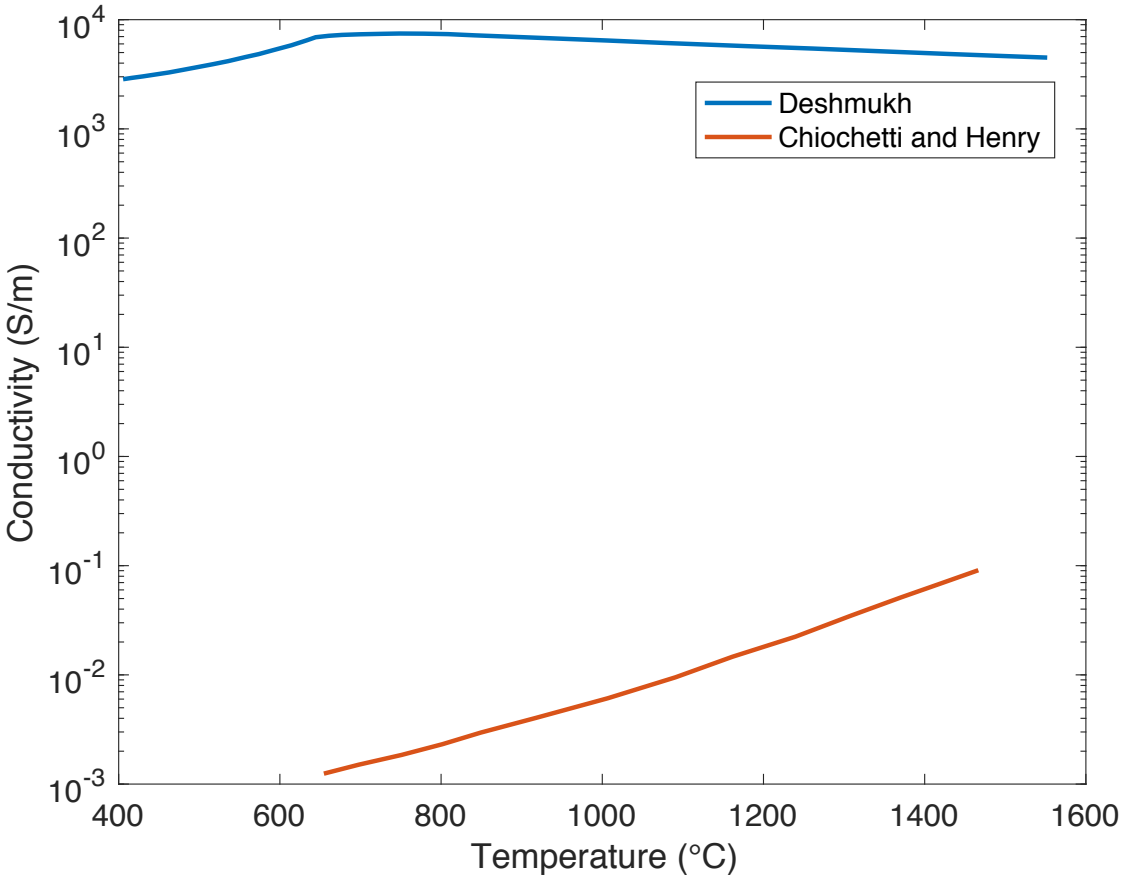

Figure 5: Plot of conductivity of silicon carbide as a function of temperature from two different sources (Deshmukh 2005; Chiochetti and Henry 1953), showing the widely different values reported in the literature.

4 Results and Discussion

4.1 Coupled electromagnetic-thermal simulation

4.1.1 Magnetic fields

A simulation was created and used to model the magnetic field generated by the induction coil, the heat generated in the firebricks, and the resulting spatial distribution and time evolution of temperature in the firebricks. Since the conductivity, σ, of the firebricks was not well known *a priori* (see Section 3.5), values of σ that gave temperature responses similar to those measured experimentally (see Section 4.2) were used. The firebrick modeled in the simulation has a diameter of 127 mm and a height of 152 mm (see Table 2).

Eqs. 11 and 12 were solved numerically using MATLAB's PDE Toolbox, which employs finite element analysis, to obtain $C(r,z)$ and $S(r,z)$, the in-phase and out-of-phase components of the magnetic stream function, respectively. Plots of $C(r,z)$ and $S(r,z)$ with a firebrick conductivity of 14 S/m are shown in Figs. 6 and 7; plots of $C(r,z)$ and $S(r,z)$ over only the firebrick region are shown in Figs. 8 and 9. Since the system is azimuthally symmetric, the solutions only had to be calculated in two dimensions on one half of the cross section of the system to fully describe the solution; to obtain the full three-dimensional picture, this solution would be revolved about the z-axis. The shape of the magnetic field lines is as expected and the partial penetration of the magnetic field into the firebrick is visible.

As expected by comparison with the results presented in Gresho and Derby (1987) and Tavakoli et al. (2009), $C(r,z)$ and $S(r,z)$ in the firebrick are largest in magnitude at the surface of the brick (the edges of the cross-section); $S(r,z)$ is of larger magnitude in the firebrick than $C(r,z)$; $C(r,z)$ is negative and $S(r,z)$ is positive in the firebrick.

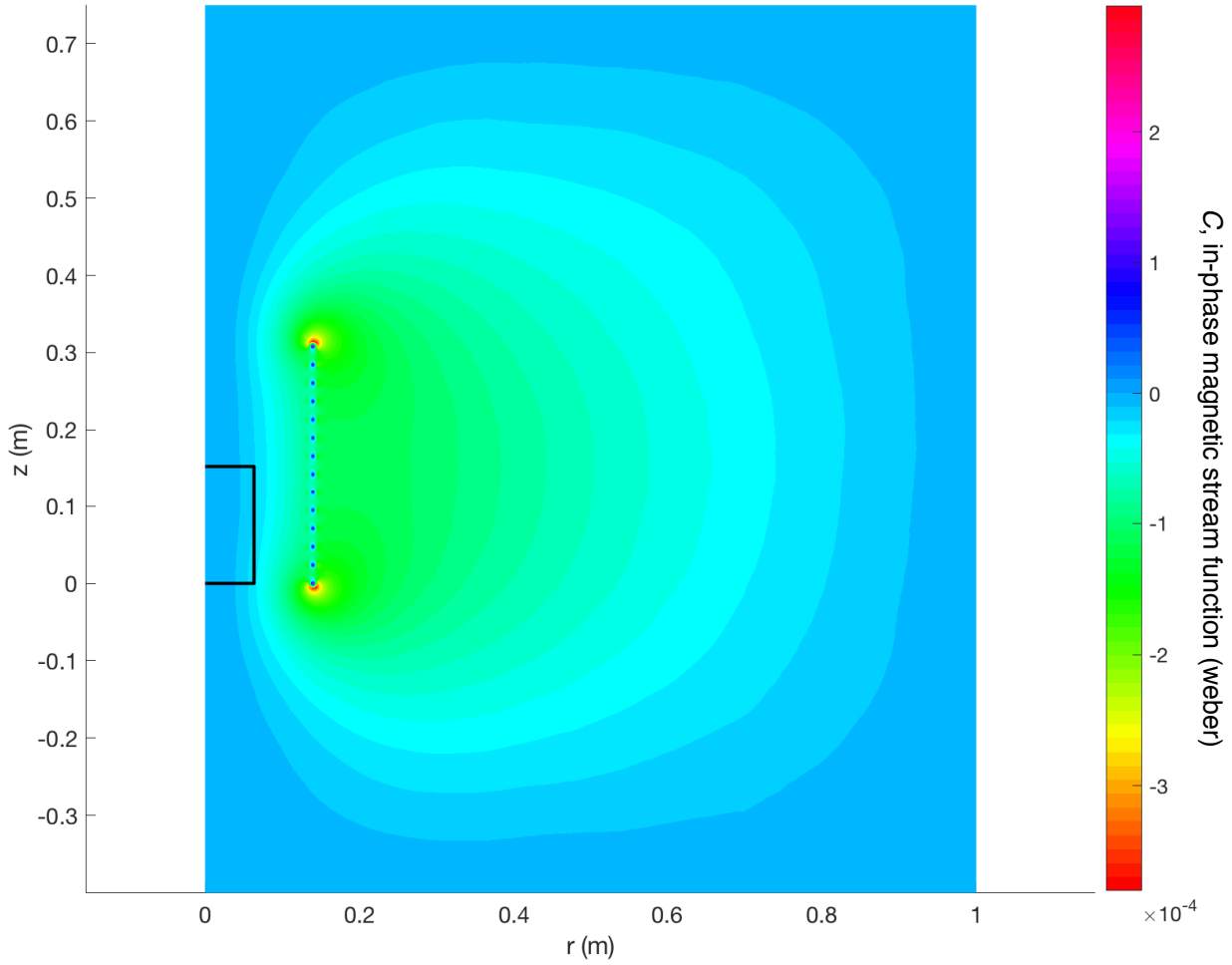

Figure 6: $C(r, z)$, the in-phase component of the magnetic stream function ψ_B, in weber. Since the solution is symmetric, only one half of the cross-section is shown. The location of the firebrick is shown by the black rectangular outline.

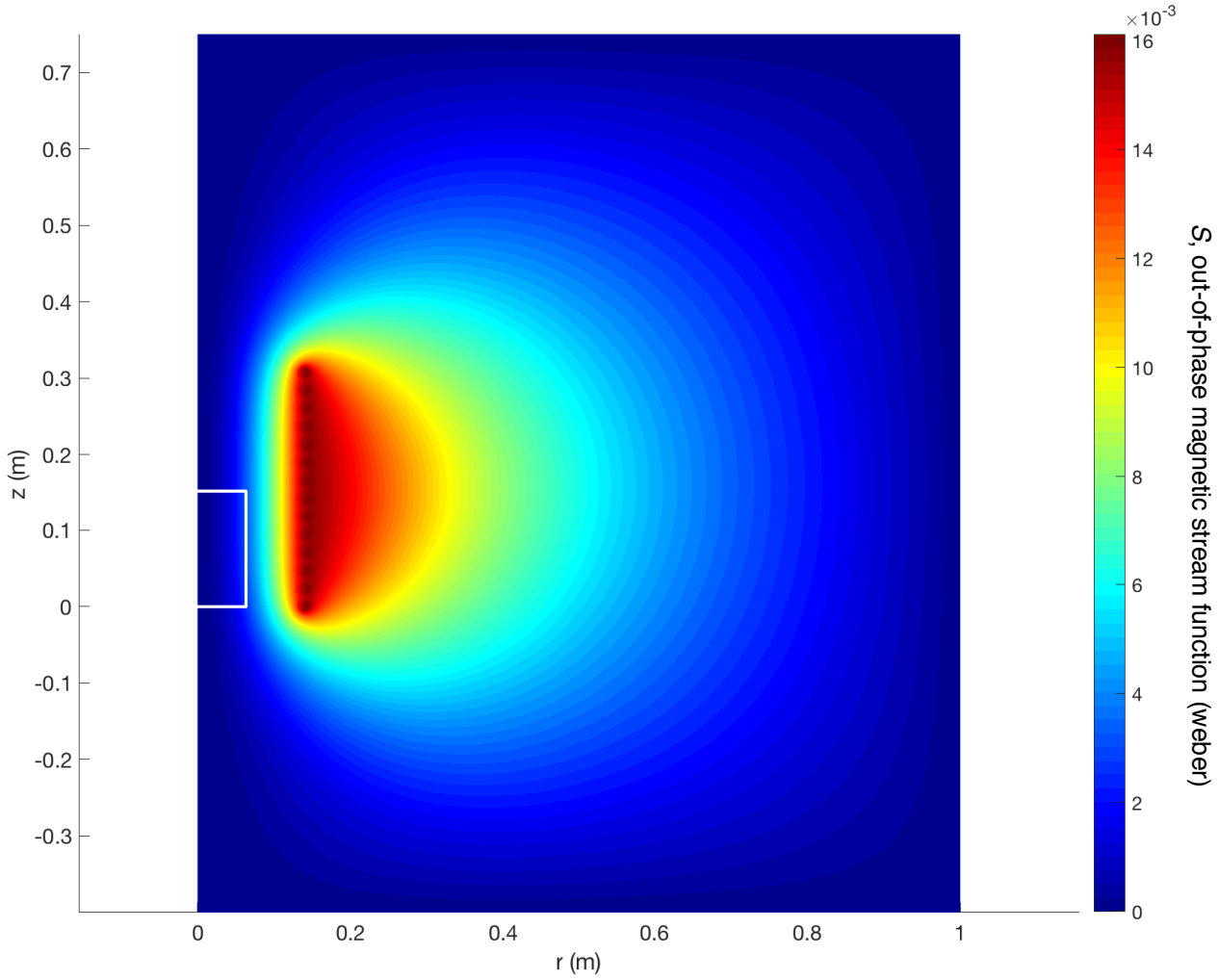

Figure 7: $S(r,z)$, the out-of-phase component of the magnetic stream function ψ_B. Since the solution is symmetric, only one half of the cross-section is shown. The location of the firebrick is shown by the white rectangular outline.

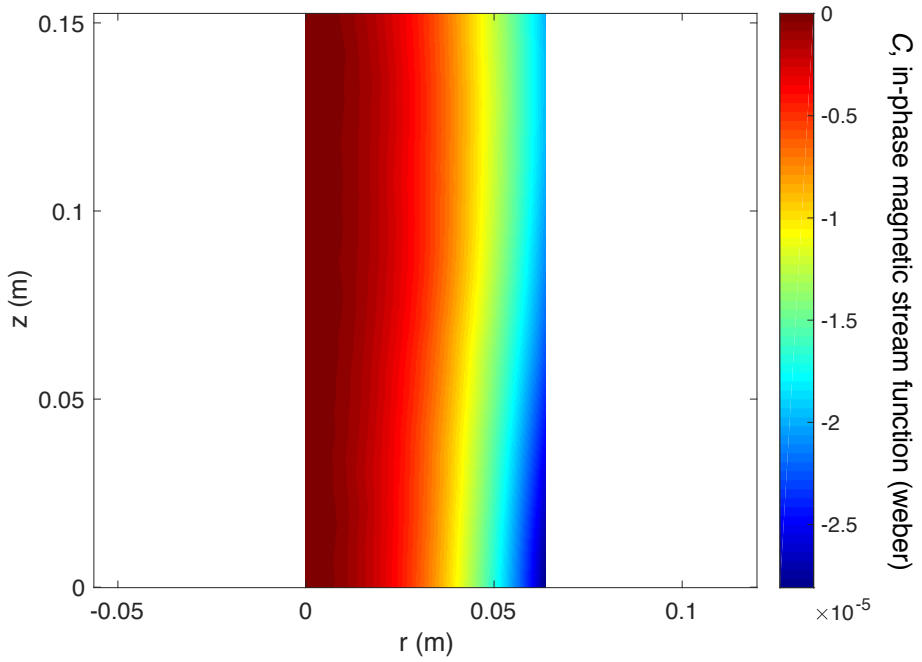

Figure 8: Close-up of $C(r, z)$ over half of the firebrick cross-section.

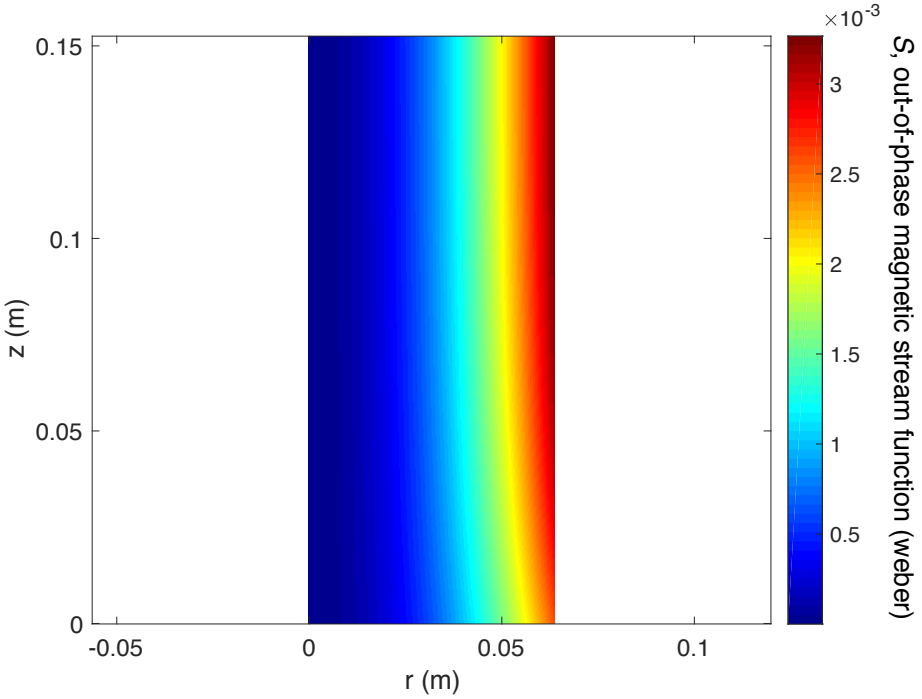

Figure 9: Close-up of $S(r, z)$ over half of firebrick cross-section.

4.1.2 Heat generation and temperature distribution

Volumetric heat generation rate $q(r,z)$ was calculated with Eq. 15 and used as the source term in the heat equation, as shown in Eq. 16. An electrical conductivity of 14 S/m was used. A plot of $q(r,z)$ is shown in Fig. 10. Maximum $q(r,z)$ occurred on the outer surface of the firebrick sample, as expected. The maximum value was 3.9×10^6 W/m^3 and the average value was 1.2×10^6 W/m^3. These values are similar to those found in Gresho and Derby (1987) and Tavakoli (2009).

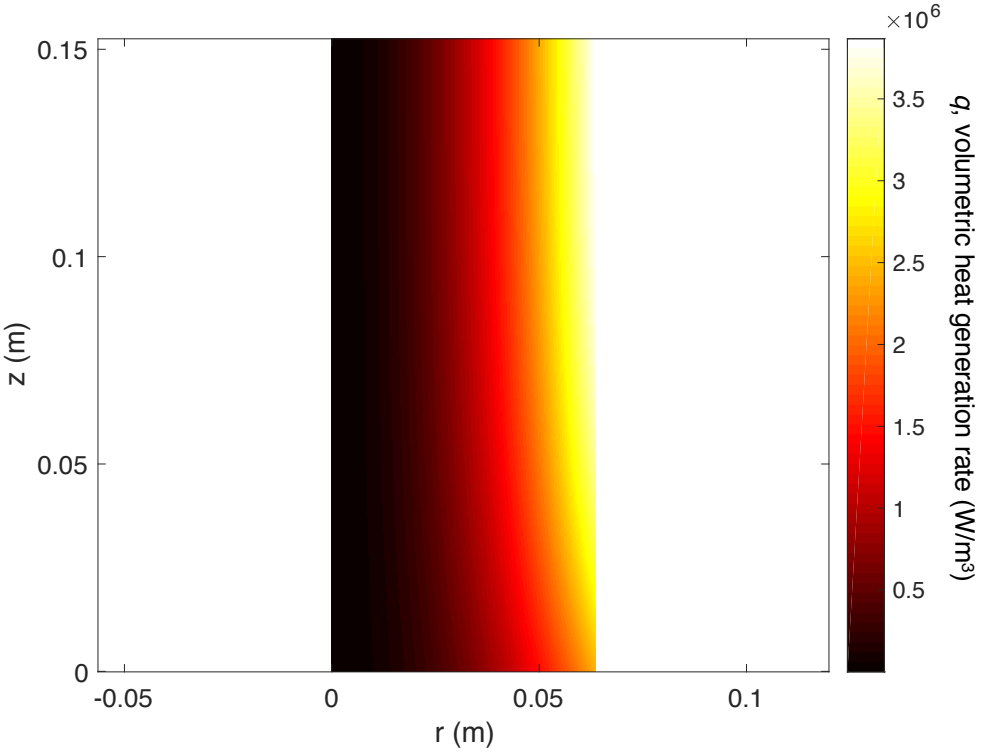

Figure 10: Plot of volumetric heat generation rate, $q(r,z)$. q_{max} = 3.9×10^6 W/m^3; q_{avg} = 1.2×10^6 W/m^3.

MATLAB's PDE Toolbox was used to numerically solve Eq. 16, with zero heat flux boundary condition at the axis of symmetry and radiative surface boundary condition with emissivity of 0.9 to account for heat loss. Steady-state temperature in the firebrick half-cross-section is shown in Fig. 11. Maximum temperature was 710°C, which occurred near the middle of the half-cross-section, and average temperature was 668°C.

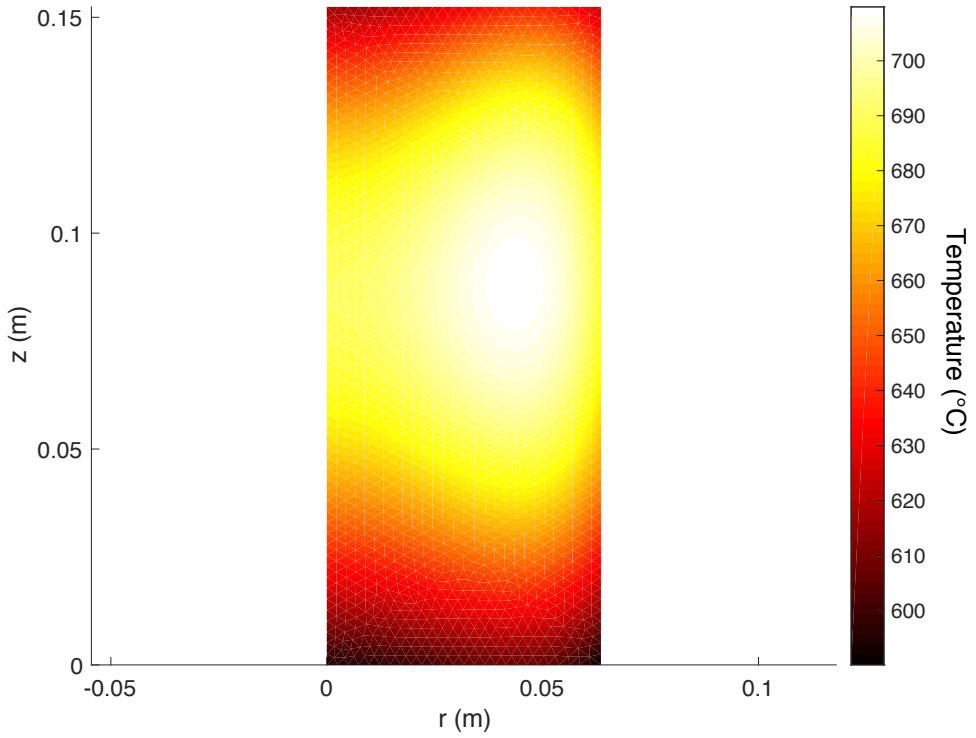

Figure 11: Plot of temperature distribution in firebrick. T_{max} = 710°C; T_{avg} = 668°C.

4.1.3 Time evolution of surface temperature

The time evolution of the temperature in the center of the top surface of the firebrick was computed, to allow comparison with experimental measurements, which were taken in the same location (see Section 3.4 and 4.2). Three different values of electrical conductivity were used, which produced three distinct temperature-time curves, as shown in Fig. 12. These curves are similar to those obtained experimentally (see Section 4.2). Direct comparison of the simulated and experimental results, as shown in Fig. 15, allows estimation of the electrical conductivity of the firebrick sample under consideration.

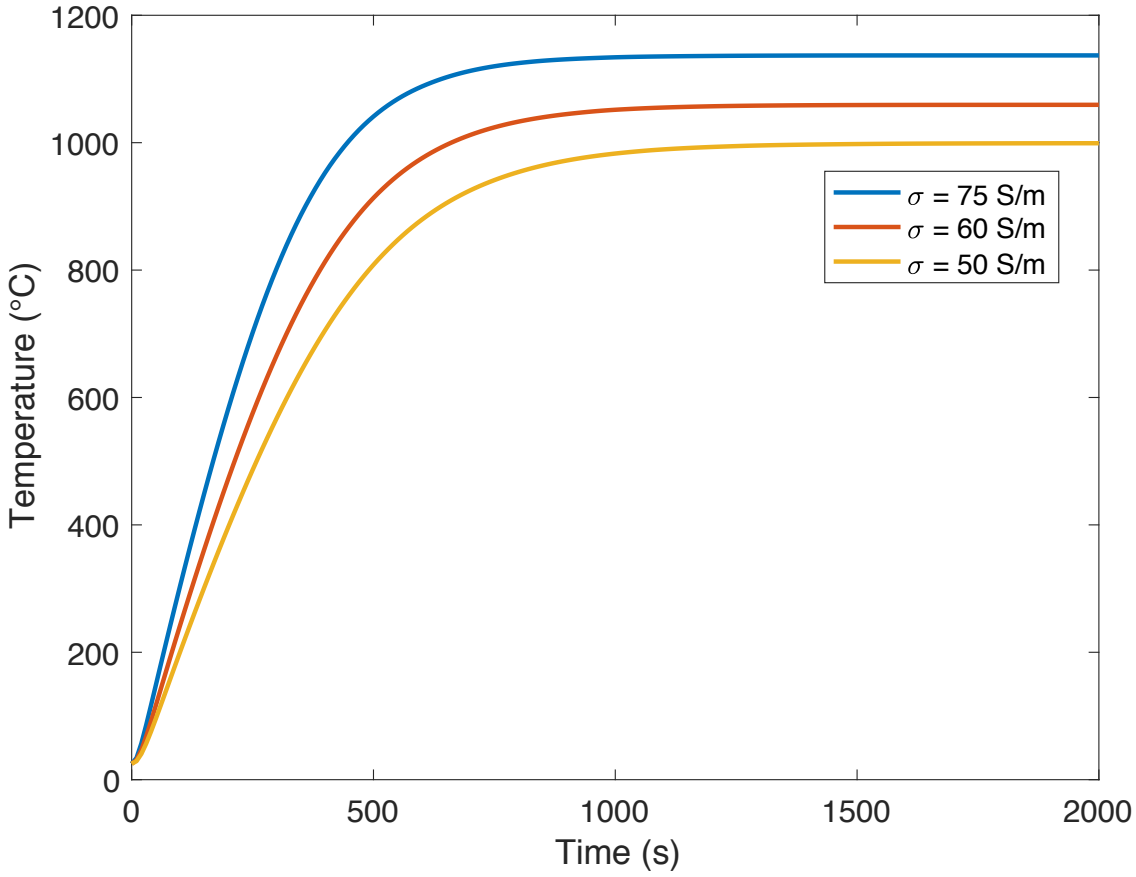

Figure 12: Plot of temperature against time with various firebrick conductivities, each producing a different curve.

4.2 Experimental temperature measurements

Five of the seven firebricks (HARBIDE, NISIC 20, SHOT-TECH SIC 80, SERV 95, TZB) coupled sufficiently with the induction furnace's magnetic field to reach temperatures above the 92°C threshold of the infrared camera. These five firebricks reached temperatures sufficiently high that they glowed visibly red, as shown in Fig. 13. Plots of the temperature response against time are shown in Fig. 14. Three of the bricks reached a temperature of 727°C, at which point the experiment was stopped. These bricks would be appropriate for the firebrick energy storage medium. The other two firebricks (GREENCAST-90 RB ON-LINE, THOR 60 ADTECH) did not exceed 92°C. These bricks would be appropriate for the firebrick insulating sheath around the

storage medium. The bricks that heated up most quickly had high concentrations of silicon carbide, zirconia or chromium oxide. However, a direct correlation between rate of temperature increase and percentage content of any particular material was not found.

Fitting simulated to experimental results, as shown in Fig. 15, allowed the average electrical conductivity of the NISIC 20 firebrick to be estimated as 14 S/m. The conductivity of this brick lies in the middle of the region between the two reported silicon carbide conductivities in Fig. 5. Similar analysis could be carried out for the other firebricks.

Using the measured rate of change of temperature in the center of the top face of the firebrick sample and assuming that temperature was uniform throughout the brick gives an estimated volumetric heat generation rate for the NISIC 20 sample of 7.7×10^5 W/m^3. However, the simulation shows that significant temperature gradients existed within the sample (see Fig. 11); this leads to a higher estimate of average volumetric heat generation rate of 1.2×10^6 W/m^3 (see Section 4.1.2). This corresponds to a total heat generation rate of 2.6 kW. Given the electrical power delivered to the induction coil of 55 kW, this corresponds to a heating efficiency of 4.7%. Efficiency might be increased by heating a larger sample.

It was thought that the firebricks might fracture due to internal stresses caused by excessive power input, so in preliminary experimental runs, the power delivered to the induction coil was not immediately set to its maximum value but was increased gradually. No fracture occurred in these preliminary runs. Neither did fracture occur in subsequent runs in which power was turned to maximum immediately; the temperature responses shown in Fig. 14 are all with power set to maximum immediately. It is thought that repeated thermal cycling might weaken the firebricks. In future work, each sample would therefore be repeatedly heated and cooled and inspected for evidence of cracking or fracturing.

Each firebrick had a unique temperature response profile, suggesting that induction heating could be used to distinguish between different firebrick compositions. For example, induction heating could be used as a quality assurance technique at a full-scale firebrick energy storage facility. Ensuring consistency of the electrical and thermal properties of the firebrick being installed will be important for ensuring optimal performance of the system. After receiving a shipment of firebrick, the facility could inductively heat firebrick samples using an experimental setup similar to that described in Section 3.4 and measure the temperature response of the samples, comparing the temperature response to that from a temperature response calibration curve. Firebrick with a temperature response curve deviating from the calibration curve by more than the

desired tolerance would be rejected. The advantage of using this approach is its simplicity (there was no need to attach instruments physically to the samples) and speed (there was virtually no setup time and the runs were each completed in less than 40 minutes).

Figure 13: A firebrick sample (composition “TZB”) at approx. 730°C during an induction heating experiment. The brick is visible at the lower edge of the top of the crucible and is glowing red hot.

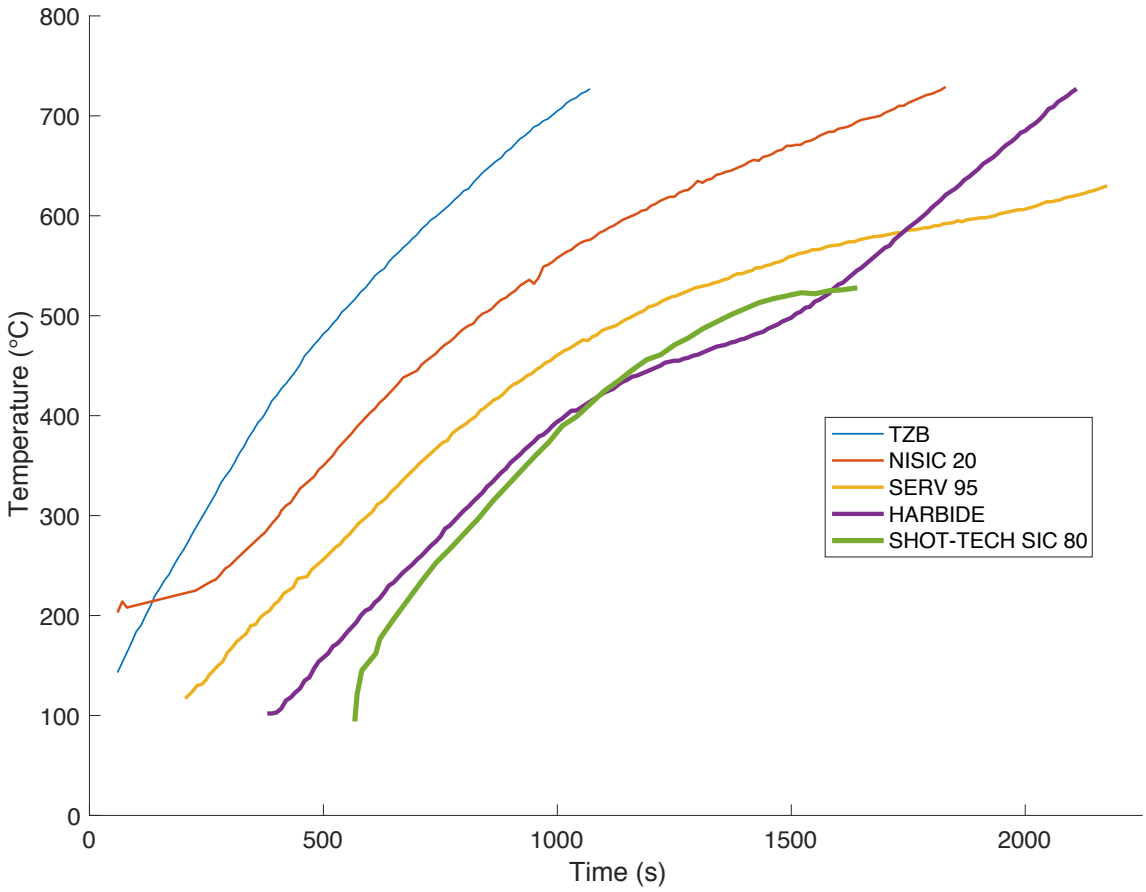

Figure 14: Plots of temperature against time for various firebricks under induction heating. Note that the plots begin at 92°C, the minimum temperature measurable with the infrared camera. Two of the bricks tested (compositions "GREENCAST-90 RB ON-LINE" and "THOR 60 ADTECH") did not couple as effectively as these bricks, reaching maximum temperatures below the 92°C threshold, but above 100°C.

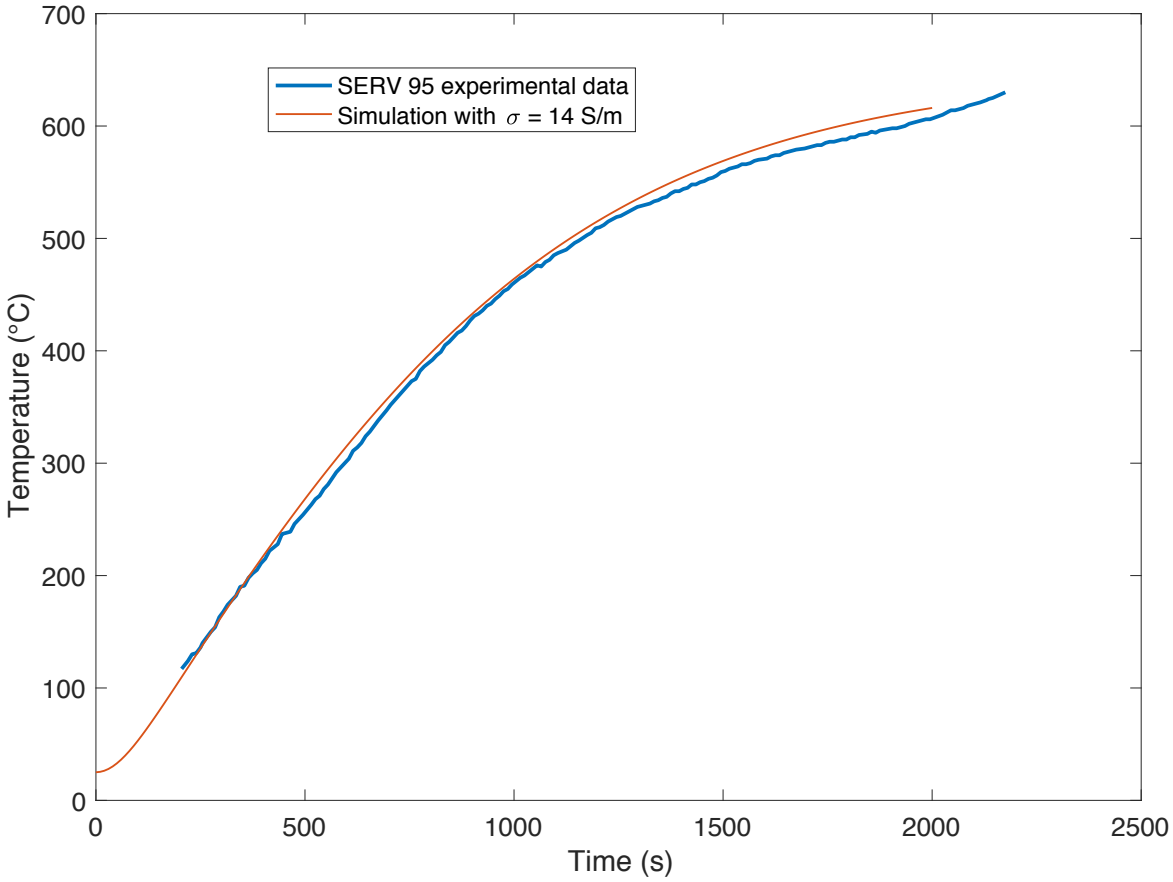

Figure 15: Plot of temperature (recorded in the center of the top face of the firebrick sample) against time, overlaying the experimental results for SERV 95 firebrick with simulated results with electrical conductivity σ of 14 S/m. The simulation can therefore be used as a way of measuring electrical conductivity.

5 Conclusion and Future Work

This work has shown that firebrick can be induction heated to high temperatures (>700°C). Numerical simulations were performed to model the distribution of magnetic fields, volumetric heat generation rate from induced eddy currents, and temperature as a function of space and time. Experiments showed that firebricks with different material compositions had different temperature response curves, showing that temperature response could be used as a way of distinguishing between different firebrick material compositions for quality assurance. The simulations showed that temperature response was positively correlated with electrical conductivity, showing that induction heating can be used as a method for measuring the electrical conductivity of firebrick materials.

In future work, the firebrick samples would be manufactured with shafts for temperature probes to allow measurement of internal temperature, which the simulations show was higher than surface temperature. More experiments would be conducted with new materials containing higher concentrations of silicon carbide, zirconia and chromium oxide to find compositions with optimal volumetric heat generation rate.

6 Appendix

6.1 Technical drawings

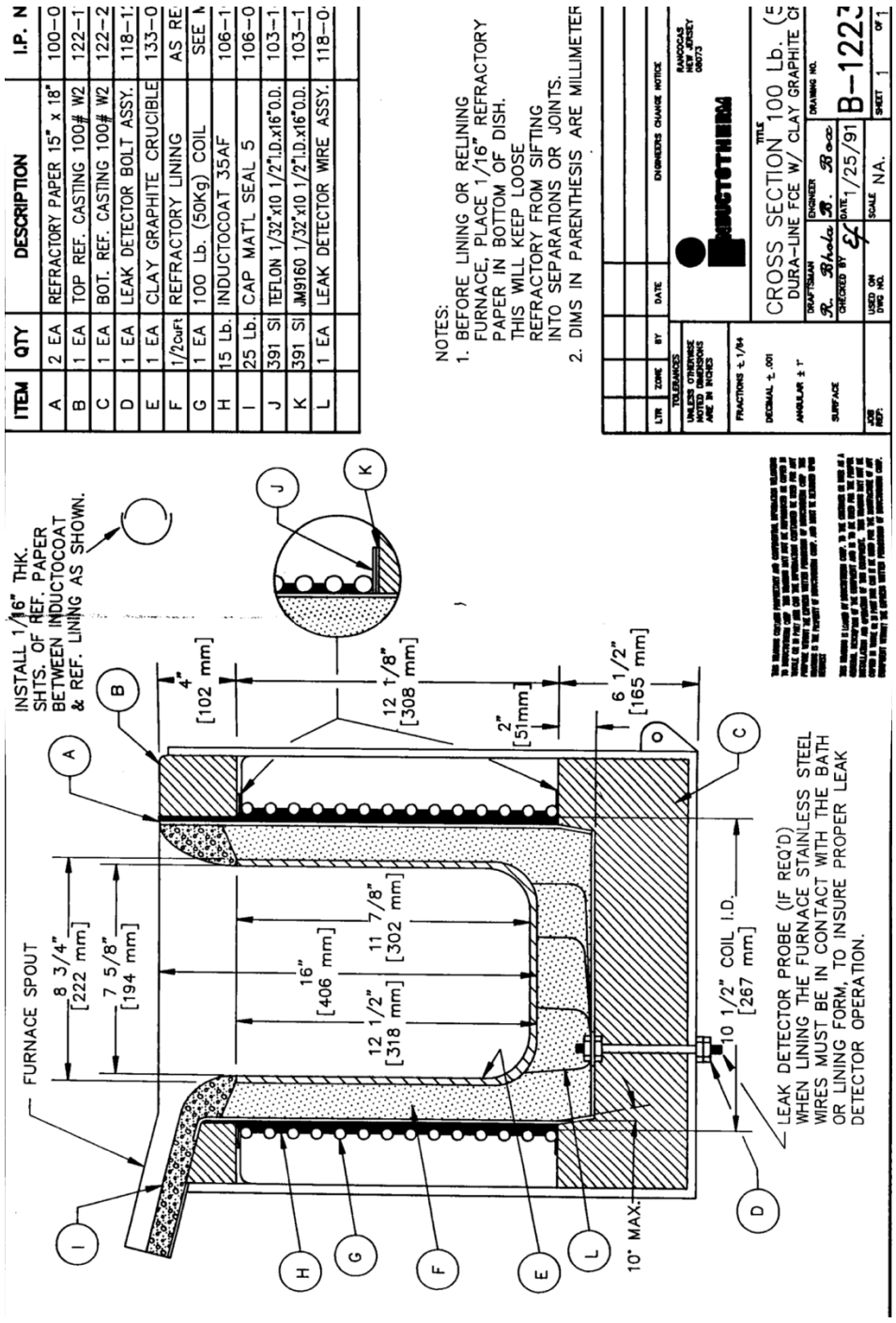

Figure 16: Technical drawing produced by the manufacturer of the Inductotherm furnace used for induction heating of firebrick samples.

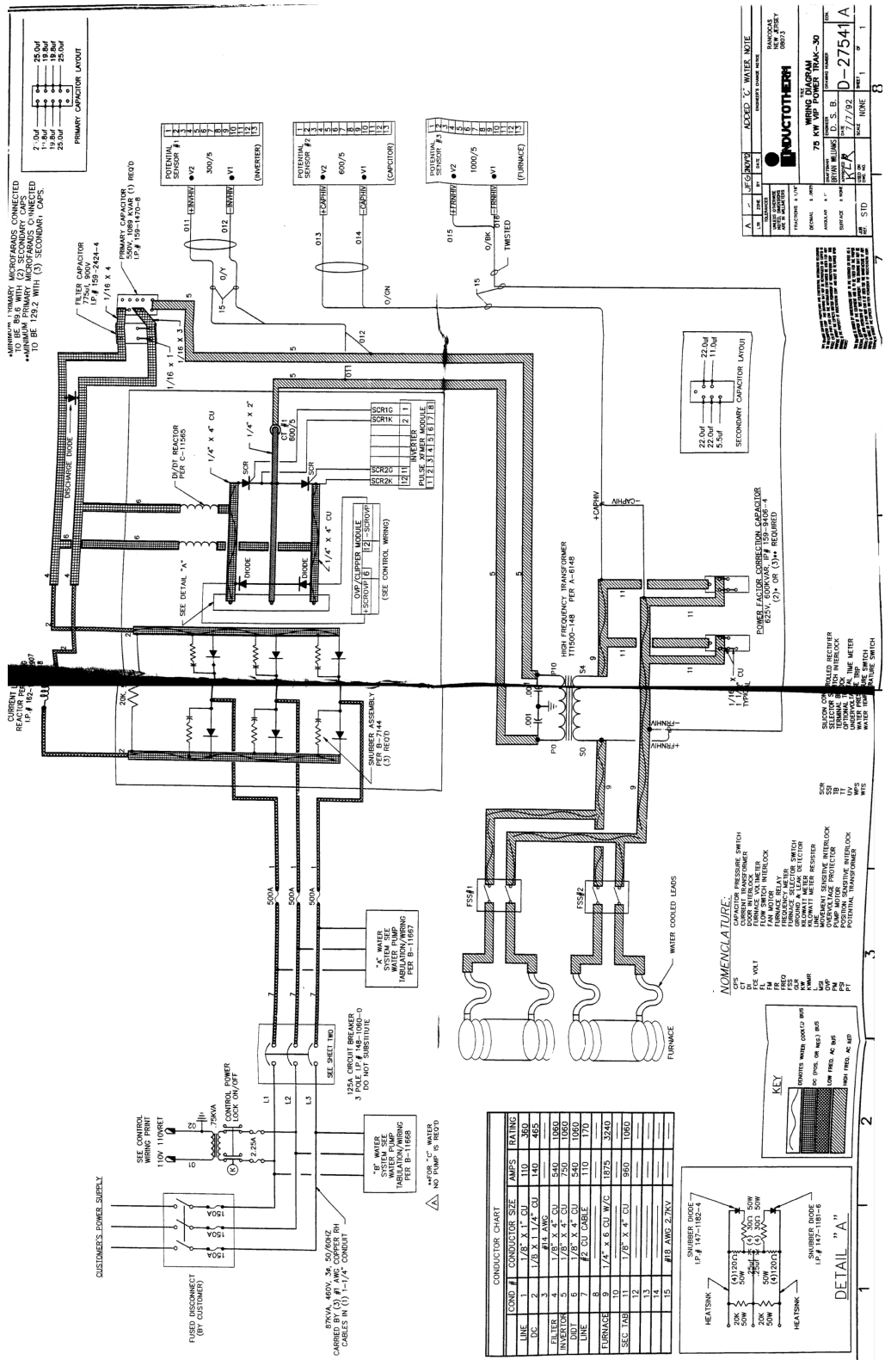

Figure 17: Circuit diagram of the Inductotherm Power-Trak 75-30 R furnace power supply.

6.2 Simulation code

```
% Induction heating model

%%%%% Define parameters used in this code %%%%%

H_fi = 6*2.54/100;          % Height of firebrick cylinder (m)
R_fi = 0.5*5*2.54/100;      % Radius of firebrick cylinder (m)
H_co = 12.125*2.54/100;     % Height of coil (m)
R_i_co = 0.5*10.5*2.54/100; % Inner radius of coil (m)
r_co = 0.5*0.5*2.54/100;    % Radius of induction coil wire (m) (= 0.25 inch)

V_coil = 900;            % Voltage across induction coil (V)
N = 14;                  % Number of turns in induction coil (dimensionless)

mu_0 = 4*pi*1e-7;     % Permeability of free space (H/m)
mu_fi = 1*mu_0;       % Permeability of firebrick (H/m)
mu_co = 1*mu_0;       % Permeability of coil (H/m)
sigma_fi = 14;        % Conductivity of SiC firebrick (S/m) at 1100 degC
sigma_co = 5.9e7;                       % Conductivity of copper coil (S/m)
omega = 2*pi*2300;                      % Frequency (rad/s)
J_0 = sigma_co*V_coil/(2*pi*r_co*N);    % Current density in coil (A/m^2)

k_fi = 3.8;                             % Thermal conductivity (W/m-K)
rho_fi = 2700;                          % Mass density of firebrick (kg/m^3)
c_fi = 750;                             % Specific heat capacity (J/kg-K)

%%%%% End of parameter definition section %%%%%



%%%%% Define geometry in PDE Toolbox (for half of cross-section) %%%%%

% Rectangle is code 3, with 4 sides, followed by x-coordinates and then
% y-coordinates
R1 = [3,4,0,1,1,0,-0.4,-0.4,0.75,0.75]'; % Creates a large rectangle
                                         % representing surrounding space
R2 = [3,4,0,R_fi,R_fi,0,0,0,H_fi,H_fi]'; % Creates a small rectangle
                                         % representing firebrick cylinder

% Circle is code 1, center (x,y), radius R, i.e., [1,x,y,R]
    % and pad Ci with zeros to enable concatenation with Ri

     % One circle for each turn of the induction coil, evenly spaced:
     C1 = [1, R_i_co+r_co, 0, r_co, zeros(1,6)]';
     C2 = [1, R_i_co+r_co, H_co/13, r_co, zeros(1,6)]';
     C3 = [1, R_i_co+r_co, H_co/13*2, r_co, zeros(1,6)]';
     C4 = [1, R_i_co+r_co, H_co/13*3, r_co, zeros(1,6)]';
     C5 = [1, R_i_co+r_co, H_co/13*4, r_co, zeros(1,6)]';
     C6 = [1, R_i_co+r_co, H_co/13*5, r_co, zeros(1,6)]';
     C7 = [1, R_i_co+r_co, H_co/13*6, r_co, zeros(1,6)]';
     C8 = [1, R_i_co+r_co, H_co/13*7, r_co, zeros(1,6)]';
     C9 = [1, R_i_co+r_co, H_co/13*8, r_co, zeros(1,6)]';
     C10 = [1, R_i_co+r_co, H_co/13*9, r_co, zeros(1,6)]';
     C11 = [1, R_i_co+r_co, H_co/13*10, r_co, zeros(1,6)]';
     C12 = [1, R_i_co+r_co, H_co/13*11, r_co, zeros(1,6)]';
```

```
    C13 = [1, R_i_co+r_co, H_co/13*12, r_co, zeros(1,6)]';
    C14 = [1, R_i_co+r_co, H_co/13*13, r_co, zeros(1,6)]';

% Geometry formed of surrounding space, firebrick and induction coils:
geom = [R1,R2,C1,C2,C3,C4,C5,C6,C7,C8,C9,C10,C11,C12,C13,C14];

% Names for the geometry objects:
ns =
(char('R1','R2','C1','C2','C3','C4','C5','C6','C7','C8','C9','C10','C11','C12
','C13','C14'))';

% Set formula:
sf = 'R1+R2+C1+C2+C3+C4+C5+C6+C7+C8+C9+C10+C11+C12+C13+C14';

% Create geometry
gd = decsg(geom,sf,ns);

%%%%% End of geometry definition section %%%%%

model = createpde(2);
geometryFromEdges(model,gd);
pdegplot(model,'EdgeLabels','on','SubdomainLabels','on'); axis equal;

% Definition of PDE coefficients
f_coil = @(region,state) [-mu_co*(J_0 -
sigma_co*omega.*state.u(2,:)./region.x);...
    -mu_co*sigma_co*omega.*state.u(1,:)./region.x];
f_firebrick = @(region,state)
[mu_fi*sigma_fi*omega.*state.u(2,:)./region.x;...
    -mu_fi*sigma_fi*omega.*state.u(1,:)./region.x];
f_elsewhere = @(region,state) zeros(2, length(region.x));
c = @(region,state) 1./region.x;

% Set boundary conditions and coefficients for PDEs
applyBoundaryCondition(model,'dirichlet','Edge',[1,2,6,7,8,9],'u',zeros(1,2))
;
specifyCoefficients(model,'m',0,'d',0,'a',0,'c',c,'f',f_coil,'Face',[16,2:14]
);
specifyCoefficients(model,'m',0,'d',0,'a',0,'c',c,'f',f_firebrick,'Face',15);
specifyCoefficients(model,'m',0,'d',0,'a',0,'c',c,'f',f_elsewhere,'Face',1);

% Generate mesh, chosing an appropriating maximum mesh size Hmax
generateMesh(model,'Hmax',0.01);
pdemesh(model);
axis equal

% Choose initial conditions (1 chosen arbitarily as a reasonably small
% number)
IC = setInitialConditions(model,1);

% Solution to PDE saved to variable 'result'
result = solvepde(model);

% Solution C(r,z) and S(r,z) extracted and plotted
u = result.NodalSolution;
figure; pdeplot(model,'XYData',u(:,1), 'ColorMap','hsv'); axis equal;
set(gca,'FontSize',14); colorbar; ...
```

```
    xlabel('r (m)'); ylabel('z (m)'); hold on;
plot([0,R_fi,R_fi,0],[0,0,H_fi,H_fi],'k','LineWidth',2);
figure; pdeplot(model,'XYData',u(:,2), 'ColorMap','jet'); axis equal;
set(gca,'FontSize',14); colorbar; ...
    xlabel('r (m)'); ylabel('z (m)'); hold on;
plot([0,R_fi,R_fi,0],[0,0,H_fi,H_fi],'w','LineWidth',2);

%%%%% Thermal part of model %%%%%
thermalmodel = createpde('thermal','transient');
geometryFromEdges(thermalmodel,decsg(R2,'R2',char('R2')'));
generateMesh(thermalmodel,'Hmax',0.005);
pdemesh(thermalmodel); axis equal

thermalProperties(thermalmodel,'Face',1,'ThermalConductivity',sigma_fi, ...
    'MassDensity',rho_fi,'SpecificHeat',c_fi);

% volumetric power generation in firebrick (W/m^3):
q = @(region,state) (interpolateSolution(result, region.x, region.y, [1]).^2
...
    + interpolateSolution(result, region.x, region.y,
[2]).^2)'.*sigma_fi*omega^2./(2*(region.x).^2);

internalHeatSource(thermalmodel,q);  % Use q as heat source
thermalBC(thermalmodel,'Edge',4,'HeatFlux',0);
thermalmodel.StefanBoltzmannConstant = 5.670373E-8; % Stefan-Boltzmann
constant (W/(m^2-K^4))
thermalBC(thermalmodel,'Edge',[1,2,3],'Emissivity',0.9,
'AmbientTemperature',298); % Radiative boundary condition
thermalIC(thermalmodel, 298);        % Room temperature initial condition (K)
tlist = [0:10:2e3]; thermalresult = solve(thermalmodel,tlist);   % Time array
to compute solution over (s)
T = thermalresult.Temperature; % Temperature (K)
figure; pdeplot(thermalmodel,'XYData',T(:,end)-
273*ones(1,length(T(end,:))),'ColorMap','hot');...
    axis equal; set(gca,'FontSize',14); colorbar; xlabel('r (m)'); ylabel('z
(m)');

%%%%% End of thermal part %%%%%
```

Bibliography

Balordi, Romano. 1980. Low frequency induction heater. US4331854A, issued February 28, 1980.

Chiochetti, V. E. J., and E. C. Henry. 1953. "Electrical Conductivity of Some Commercial Refractories in the Temperature Range 600° to 1500°C." *Journal of the American Ceramic Society* 36 (6): 180–84.

Deshmukh, Yeshvant V. 2005. *Industrial Heating: Principles, Techniques, Materials, Applications, and Design.* Mechanical Engineering: 191. Boca Raton, FL : Taylor & Francis/CRC Press.

Forsberg, Charles W., Daniel C. Stack, Daniel Curtis, Geoffrey Haratyk, and Nestor Andres Sepulveda. 2017. "Converting Excess Low-Price Electricity into High-Temperature Stored Heat for Industry and High-Value Electricity Production." *The Electricity Journal* 30 (6): 42–52.

Gresho, P. M., and J. J. Derby. 1987. "A Finite Element Model for Induction Heating of a Metal Crucible." *Journal of Crystal Growth* 85 (1): 40–48.

Hensler, J. R., and E. C. Henry. 1953. "Electrical Resistance of Some Refractory Oxides and Their Mixtures in the Temperature Range 600° to 1500°C." *Journal of the American Ceramic Society*.

Ibekwe, Richard T., and Charles W. Forsberg. 2015. "Firebrick Resistance-Heated Energy Storage: Existing Technology Base." *American Nuclear Society Transactions*.

Mohr, Gunther. 1970. "Electric Storage Heaters" 1: 30–39.

Price, A. 2011. *Energy Storage for Small and Micro Combined Heat and Power Systems*. United Kingdom: Woodhead Publishing Limited.

Rudnev, Valery, Don Loveless, Raymond L. Cook, and Micah Black. 2002. *Handbook of Induction Heating*. CRC Press.

Samsonov, G. V. 1968. *Handbook of the Physicochemical Properties of the Elements*. New York: Plenum Data Corporation.

Schmalensee, Richard. 2015. "MIT Study on the Future of Solar Energy." Massachusetts Institute of Technology.

Tavakoli, Mohammad Hossein, Hossein Karbaschi, and Feridoun Samavat. 2009. "Computational Modeling of Induction Heating Process." *Progress In Electromagnetics Research* 11: 93–102.

Virgin, George C. 1985. Electromagnetic induction air heater. US4503305A, issued March 5, 1985.